MODELLING OF THE FRACTURE PROCESS UNDER BIAXIAL LOADING

V. N. Shlyannikov*

The analytical equation for modelling the fatigue fracture processes under biaxial loading combined with an arbitrary oriented crack is suggested. The taking into account of loading biaxiality and mixed modes fracture is based on the parameter of strain energy density (SED). The method for definition of the fracture process zone size is presented and the general law of its change for different materials is obtained. A ground of the crack growth model suggested is given in comparison with experimental data for both the aluminium alloy and the steel.

INTRODUCTION

The most general deformation conditions are reached by combining a loading biaxiality and an inclined crack arbitrary orientation, and therefore one can understand that the mixed modes fracture (MMF) problems are of great interest for the specialists. The progress in solving the MMF problem may be reached by a combining both physical and mechanical approaches. In limits of mechanical models it is necessary to obtain that parameter or criterion which controls the macrolevel of crack growth. The SED-parameter can be used as a similar generalised parameter. On the microlevel one has to establish the physics of the fracture process and then to give its correspondent description. All the modern models of the crack state and growth in materials proceed from the extreme significance of fracture process zone (FPZ), in which the conditions for the damage storage and growth are created. Correlation between SED and FPZ which then is used for a modelling of the fatigue fracture processes in the most general loading conditions is shown in this work.

* Physical-Technical Institute of the Kazan Scientific Centre of the Russian Academy of Sciences

STRAIN ENERGY DENSITY PARAMETER

The total SED dW/dV may be divided into two components which are connected with elastic and plastic deformations by Sih et al. (1-4) and Lee and Liebowitz (5)

$$\frac{dW}{dV} = \left(\frac{dW}{dV}\right)_e + \left(\frac{dW}{dV}\right)_p = \frac{\sigma_o^2}{E}\left(\frac{\overline{dW}}{dV}\right)_s \qquad (1)$$

The specific dW/dV value which is the material property may be obtained over the uniaxial static deformation diagram in the true coordinates. In the SED dimensionless part $(\overline{dW/dV})_s$ one can separate the component $(\overline{dW/dV})'_s$, which in its turn is expressed through the dimensionless SED-factor S

$$\left(\frac{\overline{dW}}{dV}\right)_s = \left(\frac{\sigma_{yn}}{\sigma_o}\right)^2 \left(\frac{\overline{dW}}{dV}\right)'_s = \left(\frac{\sigma_{yn}}{\sigma_o}\right)^2 \left(\frac{\overline{S}}{\overline{\delta}}\right) = \left(\frac{\sigma_{yn}}{\sigma_o}\right)^2 \left(\frac{\overline{S}_e + \overline{S}_p}{\overline{\delta}}\right) \qquad (2)$$

Elastic-plastic analysis carried out in the whole MMF range from the normal separation to the pure shear has shown (figure 1) that for plane strain S is independent on material properties as well as on loading conditions and S = 0.21. For plane stress S is a function of the strain hardening exponent n and MMF conditions. Based on the above results the dimensionless FPZ-size δ is suggested to be determined by taking into account the equation (2) as follows

for plane strain $$\overline{\delta} = 0.21/(\overline{dW/dV})'_s \qquad (3)$$

for plane stress $$\overline{\delta} \approx [0.21+0.44\,\mathrm{Ln}(n)]/(\overline{dW/dV})'_s \qquad (4)$$

The SED-parameter is used to take into account the influence of the biaxial stress state through the correspondent criteria of equivalent stresses and strains by Birger (6) and Broude and Shkanov (7)

$$\frac{\sigma'_f \varepsilon'_f}{\sigma'_{f1} \varepsilon'_{f1}} = \frac{\eta_i^n}{b_i}(A+\gamma B)^{1-n} = \frac{1}{C} \qquad (5)$$

in which $\eta_i = (1-\eta+\eta^2)^{1/2}$, $b_i = \frac{2}{\sqrt{3}}(1+\Psi+\Psi^2)^{1/2}$,

$\Psi = (\eta-\nu)/((1-\eta\nu)$, $\eta = \sigma_{xn}/\sigma_{yn}$

$$A = \frac{2\eta_i + \sqrt{3}(\eta-1)}{2-\sqrt{3}}; \qquad B = \frac{1-\eta-\eta_i}{2-\sqrt{3}} \quad \text{for} \quad -\infty \le \eta \le 0$$

$$A = \frac{2\eta_i - \sqrt{3}}{2-\sqrt{3}}; \qquad B = \frac{1-\eta_i}{2-\sqrt{3}} \quad \text{for} \quad 0 < \eta \le 1$$

$$C = (\sigma'_{f_1}\varepsilon'_{f_1})/\sigma'_f\varepsilon'_f$$

Results of calculation by the equation (5) for different properties of material are displayed in figure 2.

RESULTS AND DISCUSSION

For modelling a fatigue crack growth under biaxial loading in the mixed modes fracture conditions the following wing equation is suggested (taking into account (2-5))

$$\frac{da}{dN} = 2a\bar{\delta}\left[\frac{\sigma^2_{yn}(\bar{S}_e+\bar{S}_p)-\sigma^2_{th}\Delta\bar{S}_{th}}{4(\sigma'_{f_1}-\sigma_m)\varepsilon'_{f_1}CE\bar{\delta}}\right]^{1/\beta} \qquad (6)$$

A ground of the equation (6) is performed in comparison with experimental data under plane strain for the cyclically stable aluminium alloy and the cyclically weakening steel and shown in figure 3. Here the full lines display results of FPZ-size calculation using experimental data of both the increment of crack length Δa and the increment of number of loading cycles ΔN. The dashed lines display calculations by the equation (6) using the FPZ-size theoretical value determined from the formulae (3). Kinetics of both the plastic zone and the fracture process zone depending on ΔN are shown in figure 4. A good agreement between the theoretical and computational-experimental FPZ values for both materials may be noticed. Unmonotonic change of the crack growth rate for a steel (figure 3,a) unlike of an aluminium alloy (figure 3,b) in the range of $da/dN \in (10^{-3}-10^{-2})$ mm/cycle is connected with the different character of the cyclic strain hardening exponent n' change for each material (figure 5). This character of n' change and as a result a change of micro- and macro-crack growth rate corresponds completely to fractographical parameters of the fracture surfaces of specimens made from a steel or an aluminium alloy. Thus, for the cyclically stable aluminium alloy during the whole extent of crack growth the ductile fracture mechanism transferred into the beach markings for $da/dN > 5\cdot10^{-4}$ mm/c is the main one. For

the cyclically weakening steel $n' \approx 1$ for $da/dN < 2 \cdot 10^{-4}$ mm/c. Moreover, the cleavage fracture mechanism is observed. For $da/dN \approx 2 \cdot 10^{-4}$ mm/cycle (when $n' > 1$) a change of fracture mechanism takes place and at $da/dN > 3 \cdot 10^{-4}$ mm/cycle the ductile beach markings will appear. Investigation carried out confirms an existence of a general law of FPZ-size δ change depending on the SED $(\overline{dW/dV})'$, which is shown in figure 6.

SYMBOLS USED

a = half crack length
n, n' = static and cyclic strain hardening exponents
E = Young's modulus
S = strain-energy density factor
$\Delta \bar{S}_{th}$ = dimensionless threshold strain-energy density factor range
δ = fracture process zone size
σ_y = yield stress
σ^o = mean stress
σ^{m}_{th} = threshold stress range corresponding to ΔK_{th} at uniaxial symmetric tension
σ_{yn} = applied stress in the y-direction
$\sigma'_f, \varepsilon'_f$ = fatigue strength and ductility coefficients at biaxial load
$\sigma'_{f1}, \varepsilon'_{f1}$ = fatigue strength and ductility coefficients at uniaxial tension
η, Ψ = biaxial stress and strain ratio
β, γ = experimental constants
ν = Poisson's ratio

REFERENCES

(1) Sih, G.C., Eng.Fract.Mech., Vol.5., 1973, pp.365-377.

(2) Sih, G.C., Int.J.Fract., Vol.10., 1974, pp.305-321.

(3) Sih, G.C. and Madenci, E., Eng. Fract. Mech., Vol.18., 1983, pp.1159-1171.

(4) Sih, G.C. and Jeong, D.Y., Theoret.Appl. Fract. Mech., Vol.14., 1990, pp.141-151.

(5) Lee, J.D. and Liebowitz, H., Eng.Fract.Mech., Vol.9., 1977, pp.765-779.

(6) Birger, I.A., Izvestija USSR Acad. Sci. Mech. Solids, Vol.4., 1977, pp.143-150.

(7) Braude, N.Z. and Shkanov, I.N., Soviet Aeronautics, Vol.27., 1984, pp.23-28.

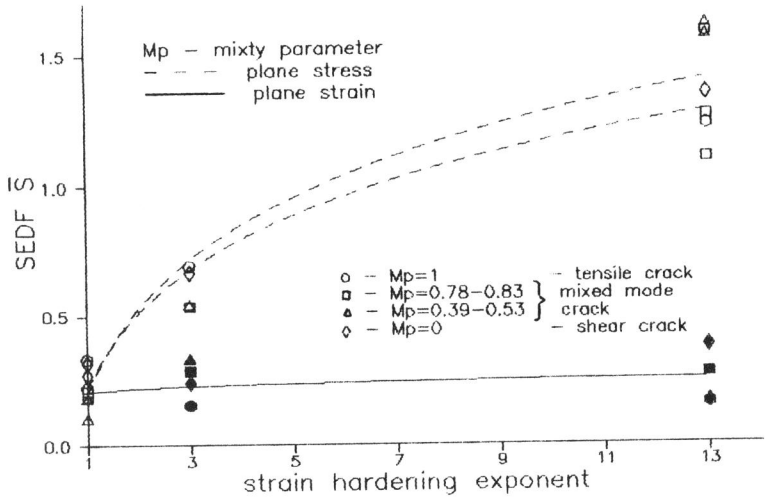

Figure 1 Values of dimensionless SEDF versus strain hardening exponent (dark point - plane strain)

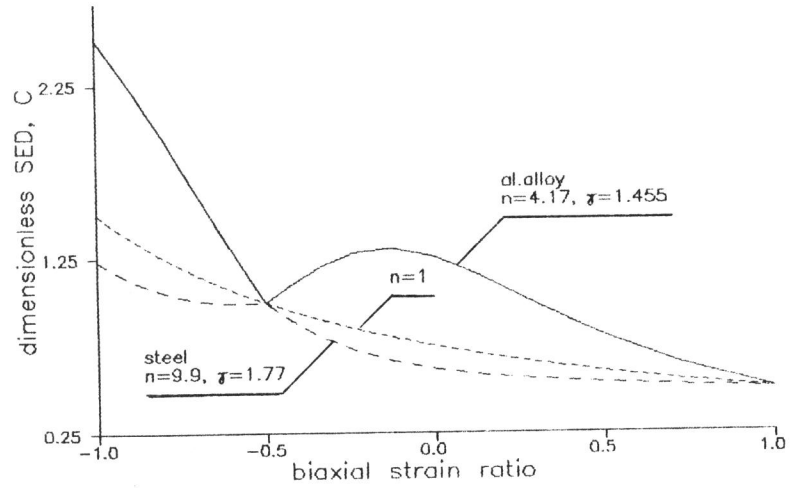

Figure 2 Dependence of dimensionless SED from biaxial strain ratio for different properties of materials

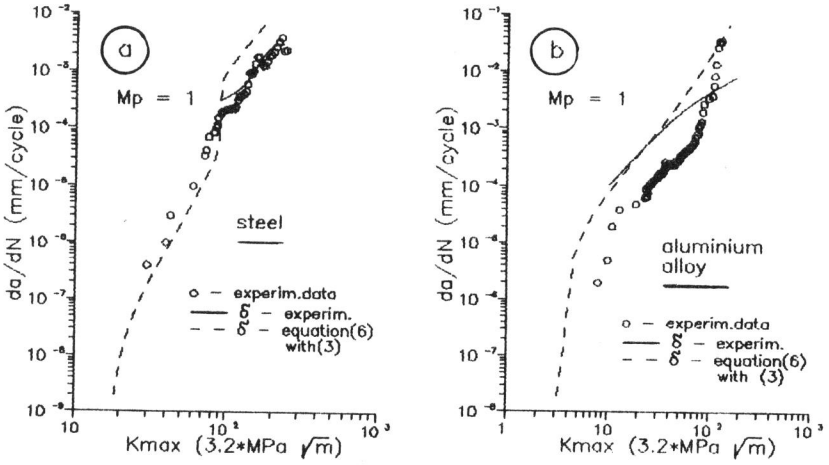

Figure 3 Comparison between the theoretical predictions and experimental data

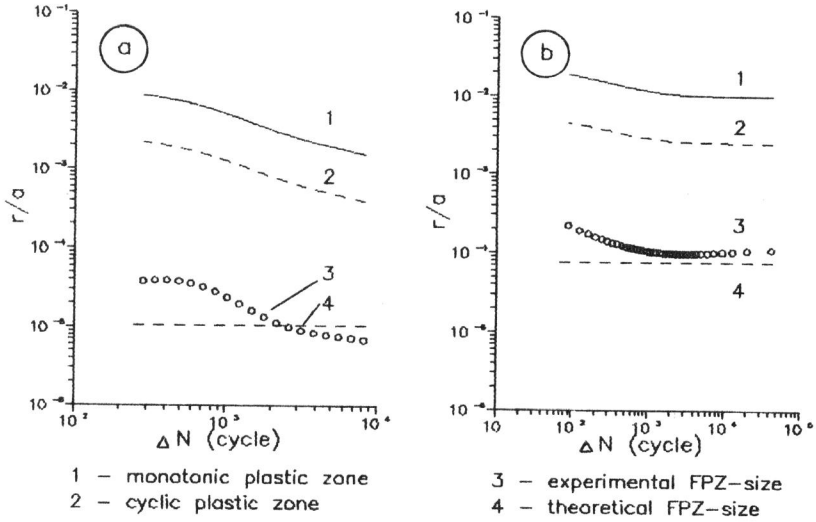

Figure 4 Kinetic of dimensionless plastic zones and fracture process zones (a - steel, b - al.alloy)

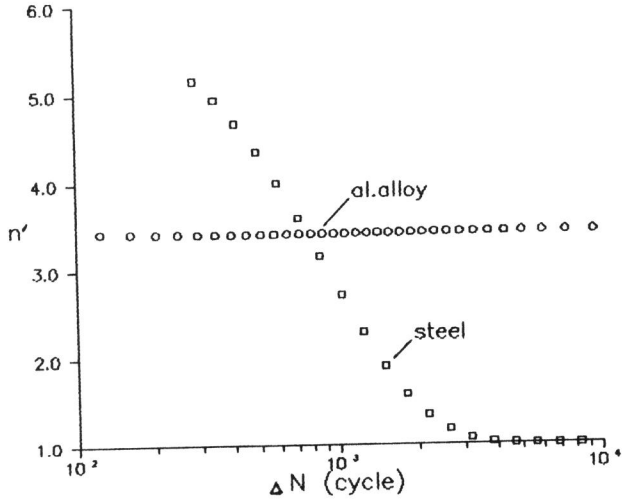

Figure 5 Kinetic of cyclic strain hardening exponent

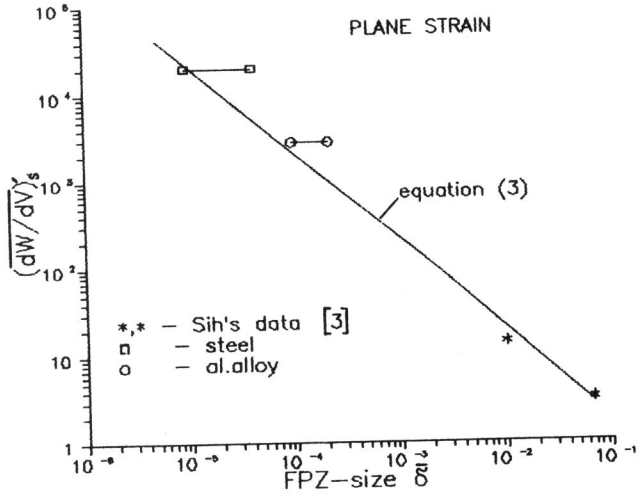

Figure 6 Strain energy density versus FPZ-size